

Fermi National Accelerator Laboratory

FERMILAB-TM-1711

**Beam Dump Designs and Muon Rates in Main
Injector Kaon Experiments**

H. T. Diehl
*Fermi National Accelerator Laboratory
P.O. Box 500
Batavia, Illinois 60510*

January, 1991



Beam Dump Designs and Muon Rates in Main Injector Kaon Experiments

H. T. DIEHL

*Fermi National Accelerator Laboratory
P.O. Box 500, Batavia, IL 60510*

ABSTRACT

A Monte Carlo study of muon fluxes from various beam dump designs for Main Injector kaon experiments was performed. The results indicate that the design goal of less than a megahertz of muons for 10^{13} incident 125 GeV/c protons is achievable.

1 Introduction

The Main Injector provides an opportunity for high statistics fixed-target kaon physics experiments. The working group Kaons at the Main Injector (KAMI) has been studying the design and physics available from a Kaon Facility experiment. This report summarizes the preliminary results of a study of the design of the beam dump.

The Main Injector is expected to deliver a primary beam containing 10^{13} 125 GeV/c protons per second. The spill is expected to be one second long with a three second cycle time.

The Kaon Facility¹ proposal has allotted 25 meters following the target to comprise the beam dump (see Figure 1). This length is constrained by the K_L^0 lifetime. The beam dump has a number of functions. They include:

1. Selecting a neutral beam and eliminating the charged hadrons including the primary (125 GeV/c) proton beam.
2. Optimizing the kaon to neutron ratio.
3. Reducing the number of photons originating at the target which exit the dump.
4. Minimizing the muon flux in the detectors downstream of the dump.

This paper describes the results of CASIM studies of muon rates in models of the Kaon Facility beam dumps at the Main Injector. The goal was to understand how to produce a collimated neutral beam with the minimum μ flux.

2 CASIM

CASIM² is a Monte Carlo program which simulates the average development of showers produced by high energy hadrons. This program was selected because it is supported by the FNAL Computing Division and because it is familiar to the FNAL Radiation Safety Group. While it measures the muon flux due to sources including prompt muons, pion decay, kaon decay, and pair production by photons, it does not take into account the muon halo around the primary beam.

3 General Aspects of Beam Dumps

An effective muon dump uses a combination of shielding and steering to decrease the muon flux in the spectrometer. Charged particles are steered by a magnetic field out of the neutral channel into the copper coils and magnet iron. Muons with momentum 1 to 100 GeV/c lose from 1 to 1.6 GeV/c of momentum for each meter of iron traversed³. Thus, low energy muons are absorbed by the dump. Muons which escape the dump have acquired enough transverse momentum due to the magnetic fields that they pass outside of the spectrometer. A Monte Carlo beam dump following the guidelines suggested above was modeled in detail.

4 The Beam Dump Models

The following constraints applied to the incident beam. The primary proton beam of 125 GeV/c was expected to be incident at a vertical targeting angle of 20 milliradians (mrad) in order to optimize the kaon to neutron ratio. The target used in these studies was a 16 cm long beryllium cylinder with 0.4 cm diameter.

The 25 meter long dump model was comprised of three sections. The first two were 7.5 meters long. The third was 10 meters long. It was divided this way for a variety of reasons. The modular approach allows for more flexibility in as far as the sections can be moved or removed depending on the needs of the experiment. For instance, a K_S^0 experiment would require only the first section. Also, the magnets used in the dump are modeled after already existing magnets which are from 5 to 7 meters long. Figure 2 shows the rough location and length of the three sections.

Following the target was a 7.3 meter long dipole magnet. The magnet was modeled after the Proton Center Hyperon Magnet, currently located at the entrance to PC4. The main features of the magnet include its large size, steel pole tips, and a removeable channel. The magnets size and the geometry of the pole tips enable it to produce a field strength up to 35 kilogauss (kG)(see Figure 3). The removable channel allows various collimator designs depending on the needs of the experiment. This magnet was selected because its strong field would sweep charged particles (including muons) into the steel and copper of the magnet as far upstream as possible. The limiting aperture of the 30 micro-steradian collimator was located in this magnet about 200 cm from the target. This was downstream of the point where the primary (125 GeV/c) protons were swept into the collimator walls. Beyond that, the details of the collimator shape were not thought to be important for this study. All of the models used this dipole magnet as the first section.

The following lists the important aspects and outlines the differences, including details of the second and third sections, of the various models tested.

1. Protons were incident on the target at an upward angle. The section 1 dipole bends horizontally. There is inert steel in the second and third sections including the two meter space between sections 2 and 3. The beam is four feet off the concrete floor.

2. Same as 1) except that the targeting angle is downward,
3. Targeting upward. Bend horizontally. Section 2 is a second dipole magnet modeled after the E8 Hyperon Magnet (shown in Figure 4). It is similar to the Proton Center Hyperon Magnet except that it does not have pointy iron pole tips. The field is about 2.5 Tesla-meters at the poles. and is parallel to and in the same direction as the field of the magnet in section 1. The third section is inert steel.
4. Same as 3) except the field of the section 2 dipole magnet is anti-parallel to the field of the first dipole magnet.
5. Same as 4) except that the last 3 meters of the section 3 magnet steel are replaced with concrete.
6. Targeting downward. Sweep vertically, with the positively charged particles swept downward in the first section. Section 2 contains a toroid spoiler magnet shown in Figure 5. This is a physically large magnet with one coil. The chief feature of this magnet is that the field of return yoke is outside of the muon flux. The field in the region of the charged particles is parallel to the field in the center of the section 1 dipole magnet. However, the field is not uniformly strong. The third section contains a 12 meters of B2 (Main Ring) dipole magnet as shown in Figure 6. The field is parallel to the field of the first section. This is surrounded by steel for the first 9 meters and concrete for the last 3 meters. The beam is eight feet off the floor.
7. The same as 6) except that the field in the second section is set to zero.

Something should be said about the magnet simulations used in this study. Field maps of the Monte Carlo magnets were produced using POISSON⁴. These field maps, which included details of the field components throughout a cross-section of the magnets were made into data files and combined with appropriate subroutines to produce adequate computer models.

5 Results and Discussion

This section describes the results of the Monte Carlo runs. CASIM outputs provided the muon spectrum and flux in a variety of different forms. The results presented here are the spectrum or total flux inside four concentric rings around the center of the neutral beam at various distances from the target. The radial boundaries of the rings are 50, 100 and 150 cm. The spectra and flux presented for region partitioned by the first ring include all muons within a circle with a radius 50 cm. The second ring contains muons from 50 to 100 cm from the center of the neutral beam. The third contains all muons from 100 to 150 cm. The fourth is all muons outside of 150 cm. Figure 7 illustrates these regions. Note that for these runs, when a muons

position exceeded 4 meters from the neutral beam center, it was considered lost and no longer traced through the model.

The muon spectrum at the end of section 1 is shown in Figure 8. This spectrum was nearly identical for all of the runs.

The purpose of the first four models was to determine the best way to use a dipole magnet in the second section and to determine whether there was an advantage in targeting upward or downward. The results are shown in Figure 9 to Figure 12. They indicated that using a dipole magnet with the field anti-parallel to the field of the section 1 dipole is the best choice. The reason is that the bulk of the muon flux is in the return yoke at section 2. Therefore, the field in the return yoke should be arranged so as to continue to bend the muons out of the beam. There was a factor of 3-10 advantage with this field geometry compared to using no field at all and a factor of ~ 50 compared with using parallel fields. With horizontal bending, the muon flux was independent of whether the beam was incident on the target from above or below.

The fifth model was a test of the effect of replacing the last three meters of the non-magnetized iron of the third section with concrete. This was thought to be a realistic change because concrete is used as an absorber of low energy neutrons. Because the density of concrete is smaller than that of iron (2.5 g/cm^3 vs 7.9 g/cm^3), and because concrete has a smaller atomic number than iron (avg. = 11 vs. 26), muons will penetrate further. It was expected that low energy muons would escape the concrete-ended dump which would be absorbed in the iron. The results are shown in Figure 13. The effect was to increase the muon flux by about a factor of three.

The sixth model was the result of trying to avoid the problems created by using a dipole magnet in the second section. That is: high energy muons which were inside the coils of the second dipole in models 4) and 5) were bent back towards the beams center. The solution was to insert a physically large magnet with a return yoke far from the muon flux. The field in the beam-channel of section 2 was parallel to that in section 1 avoiding the disadvantage of models 4) and 5). Because the return yoke is far from the beam, the serious problem of model 3) is avoided. The results are shown in Figure 14. The results of this model were similar to those of model 5) except right at the end of the dump where model 5) was about a factor of 5 more effective. Also, independent of the distance from the target, the spoiler model was $\sim 70\times$ more effective inside the region with outer boundary at 50 cm. The integrated flux inside a 1.5 meter radius circle at a distance of 3500 cm from the target is $\sim 4 \times 10^{-8}$ muons per incident proton. At 5000 cm from the target, this rate has fallen to $\sim 2 \times 10^{-8}$ muons per incident proton.

The purpose of model 7) was to see the if the effect of the small field in section 2 of the previous model was important. The results are shown in Figure 15. They indicate that operating without a magnetic field in section 2 results in an increase of a factor of 2 to 4 in the muon flux.

6 Conclusion

A variety of beam dumps have been modeled with the goal of providing a low muon flux and a flexible design. Two models stood out in the end with similarly low muon fluxes. They are three section designs with a high-field dipole magnet in the first section, and either an anti-parallel dipole magnet in the second and inert steel in the third section, or a large spoiler magnet in the second and a shielded long B2 (or similar magnet) in the third section. Monte Carlo calculations indicate that fluences of $\sim 2 - 4 \times 10^{-8}$ muons per incident proton in the KAMI spectrometer are easily reachable. With 10^{13} protons per second incident on target, these rates are below the design goal of 1 megahertz.

References

- [1] W. Molzan et al. High Sensitivity, High Precision K^0 Physics at the Main Injector. Letter of Intent P804, Fermilab, 1988.
- [2] A. Van Ginnekan. Calculation of the Average Properties of Hadronic Cascades at High Energies (CASIM). In W. R. Nelson and T. M. Jenkins, editors, *Computer Techniques in Radiative Transport and Dosimetry*, 1980.
- [3] Particle Data Group. Review of Particle Properties. *Phys. Lett.*, **204B**:1, 1988.
- [4] R. F. Holsinger and C. Iselin. The Cern-Poisson program package (POISCR). Computing Division Report PM0054, Fermilab, 1983.

Model neutral kaon apparatus using the Main Injector

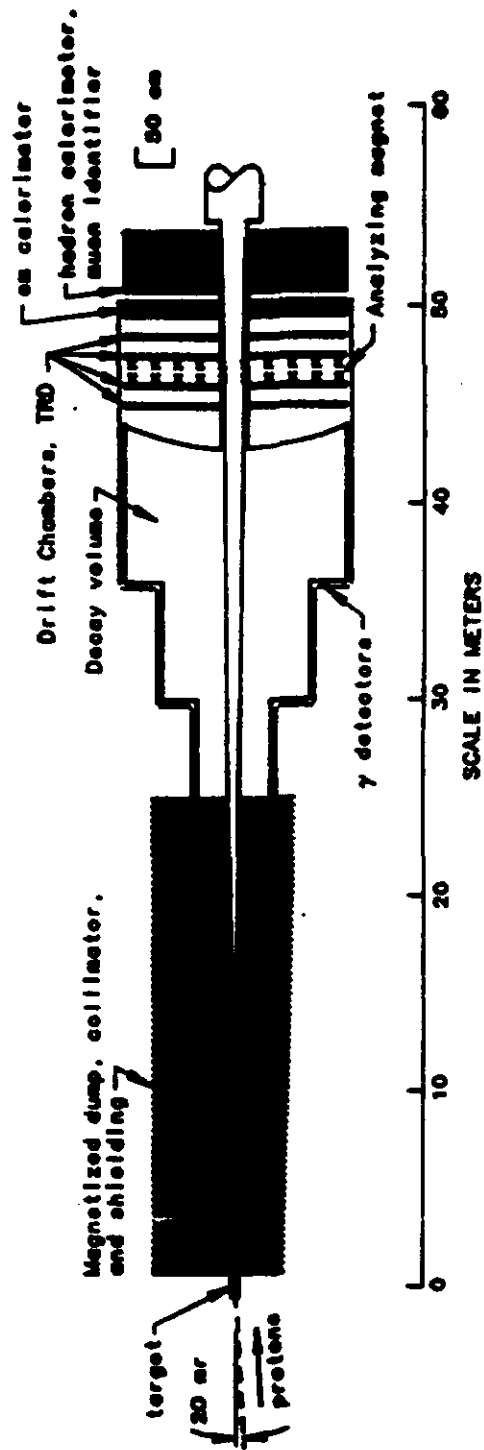


Figure 1: Picture of the kaon facility in the P-804 Letter of Intent.

Beam Dump Geometry

Basic Geometry: 125 GeV/c Protons Incident at 20 mRad

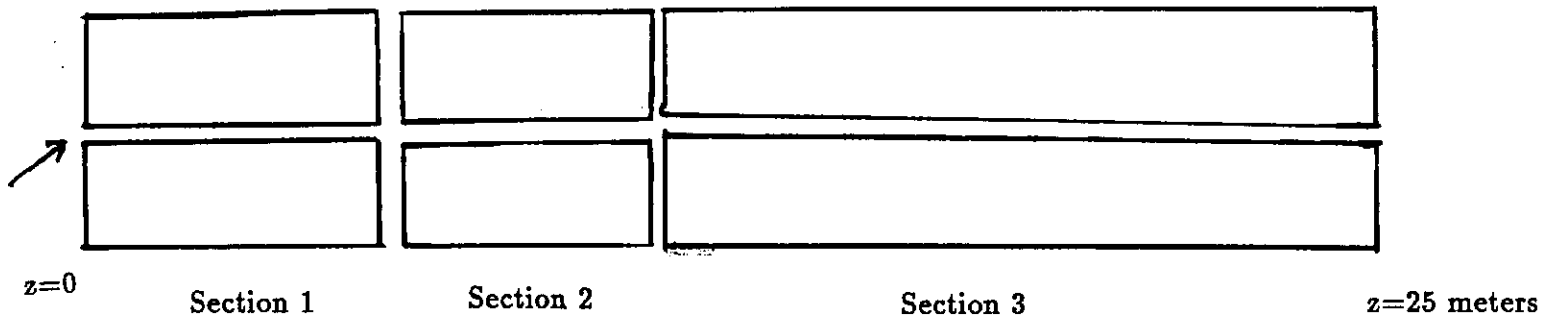


Figure 2: Three section design of the beam dump.

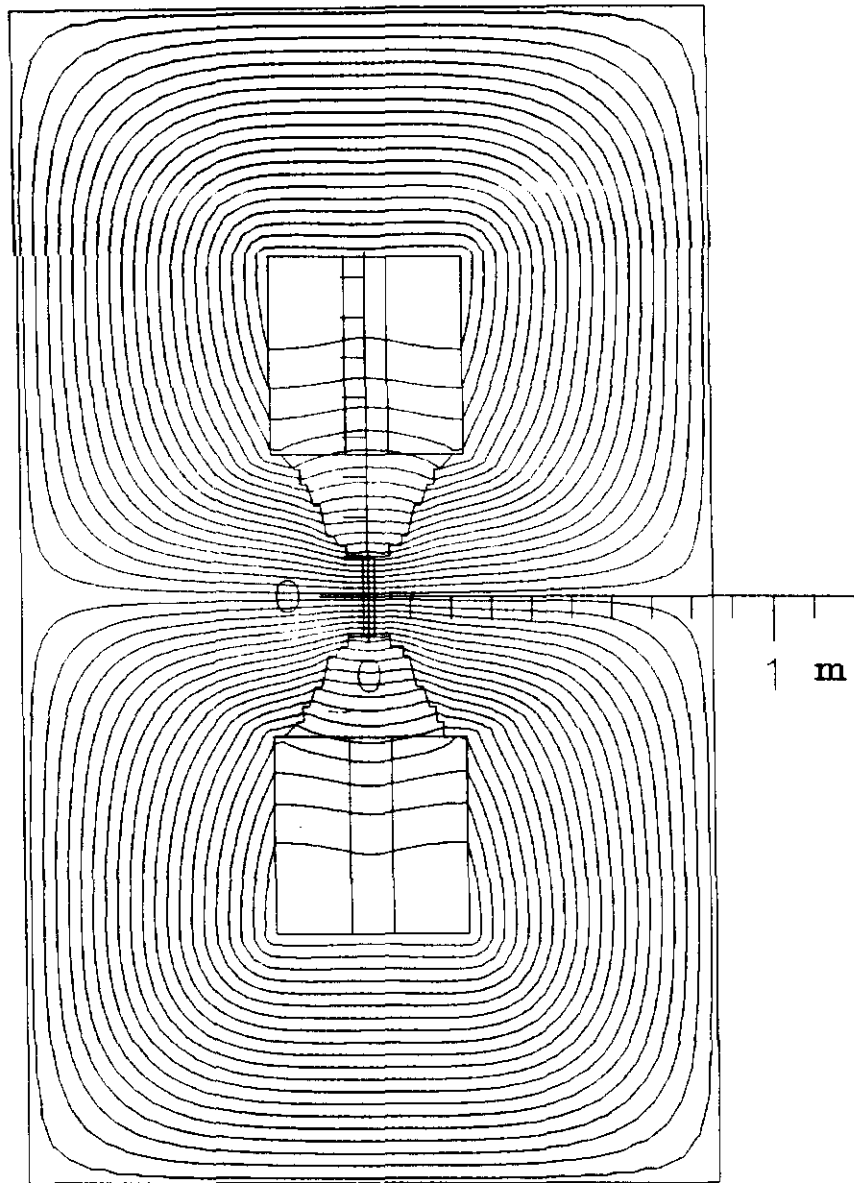


Figure 3: This figure is a cross-section of the magnet used in the first section of the three section dump. It is modeled after the PC4 Hyperon Magnet. The return yoke and poles are iron. The coils are copper. The triangular pieces between the coils and pole tips are made of lead.

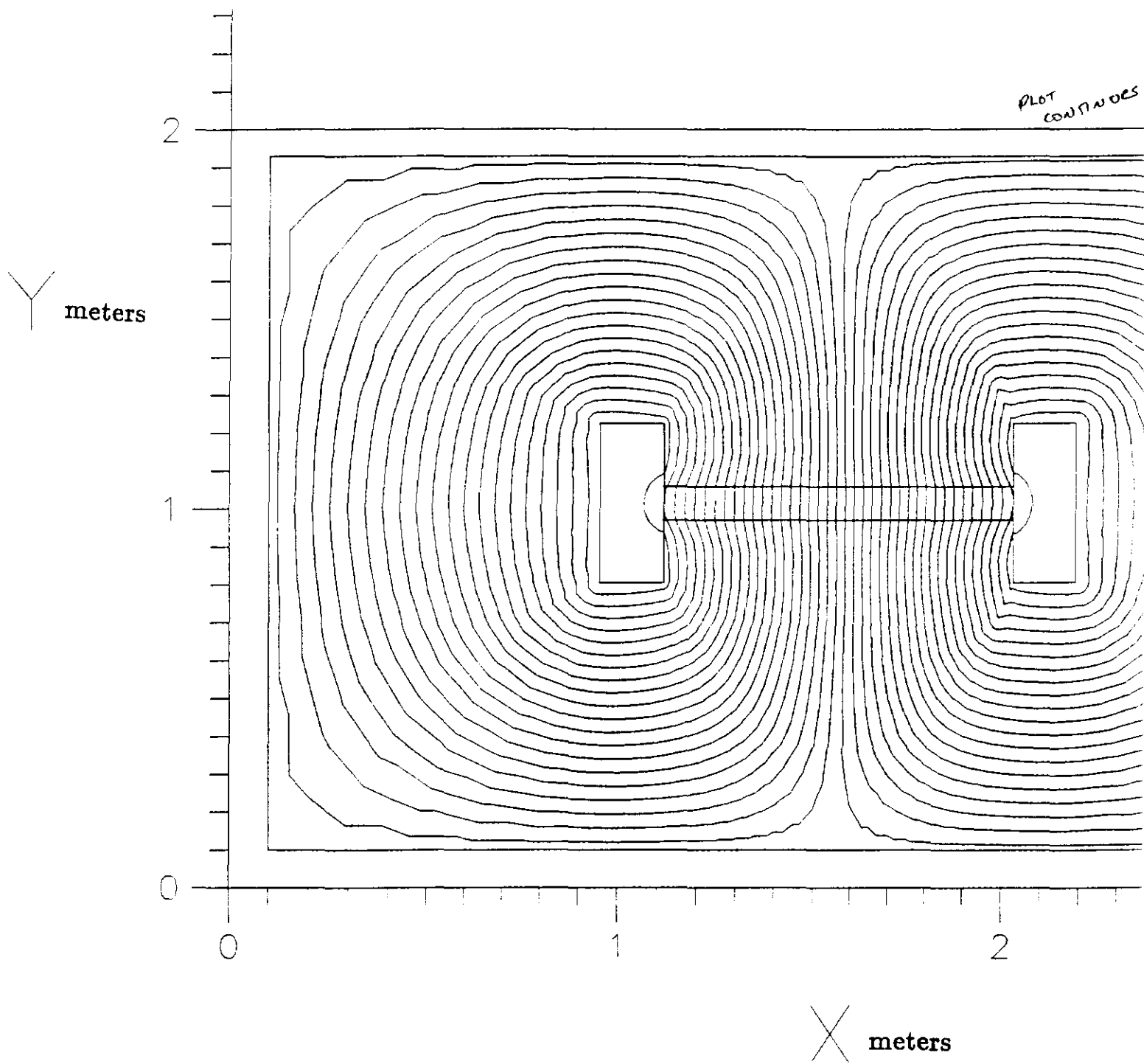


Figure 4: This figure is a cross-section of the magnet used in the second section of models 3), 4), and 5). It is modeled after the E8 Hyperon Magnet.

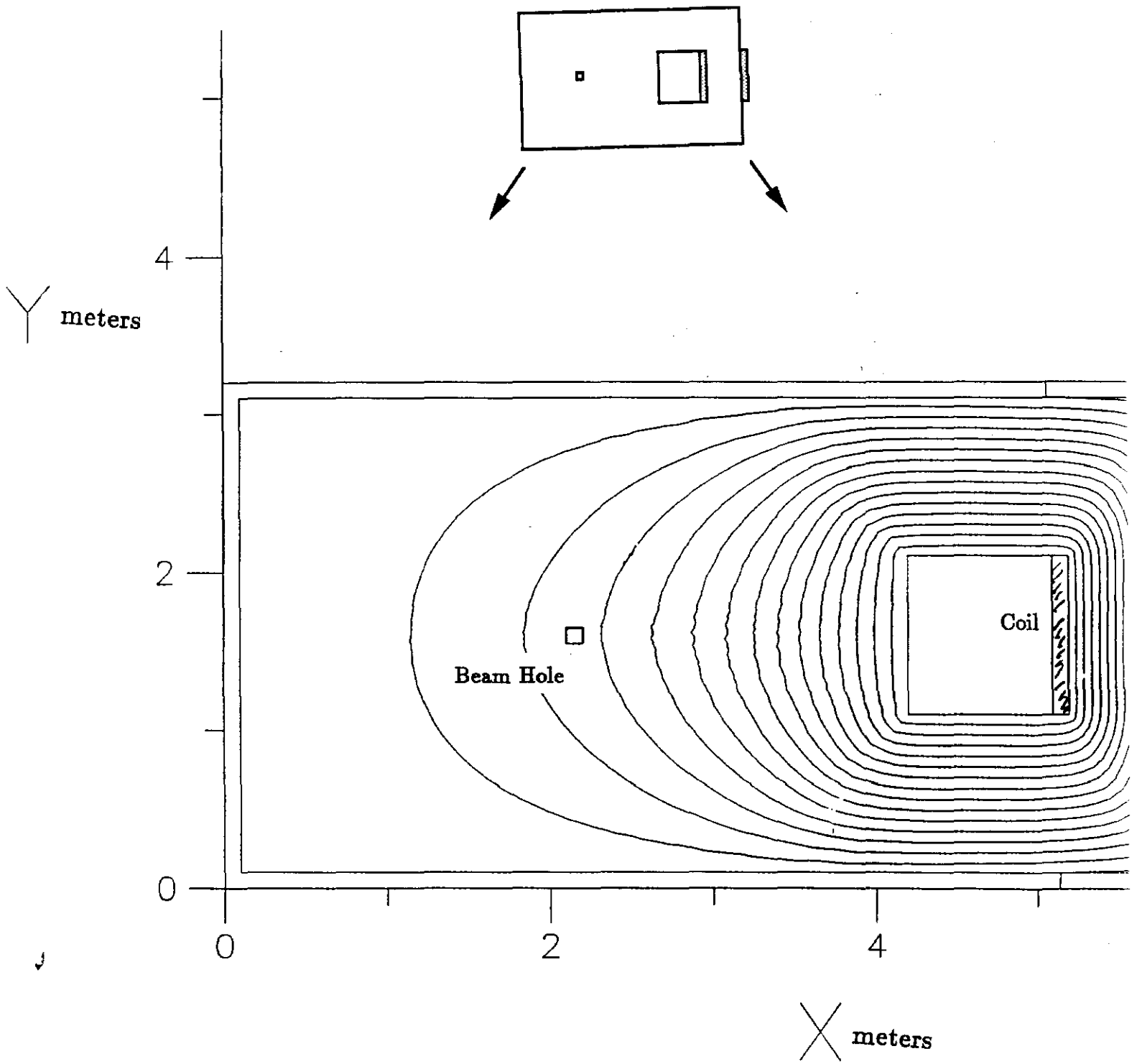


Figure 5: This figure is a cross-section of the magnet used in the second section of models 6) and 7).

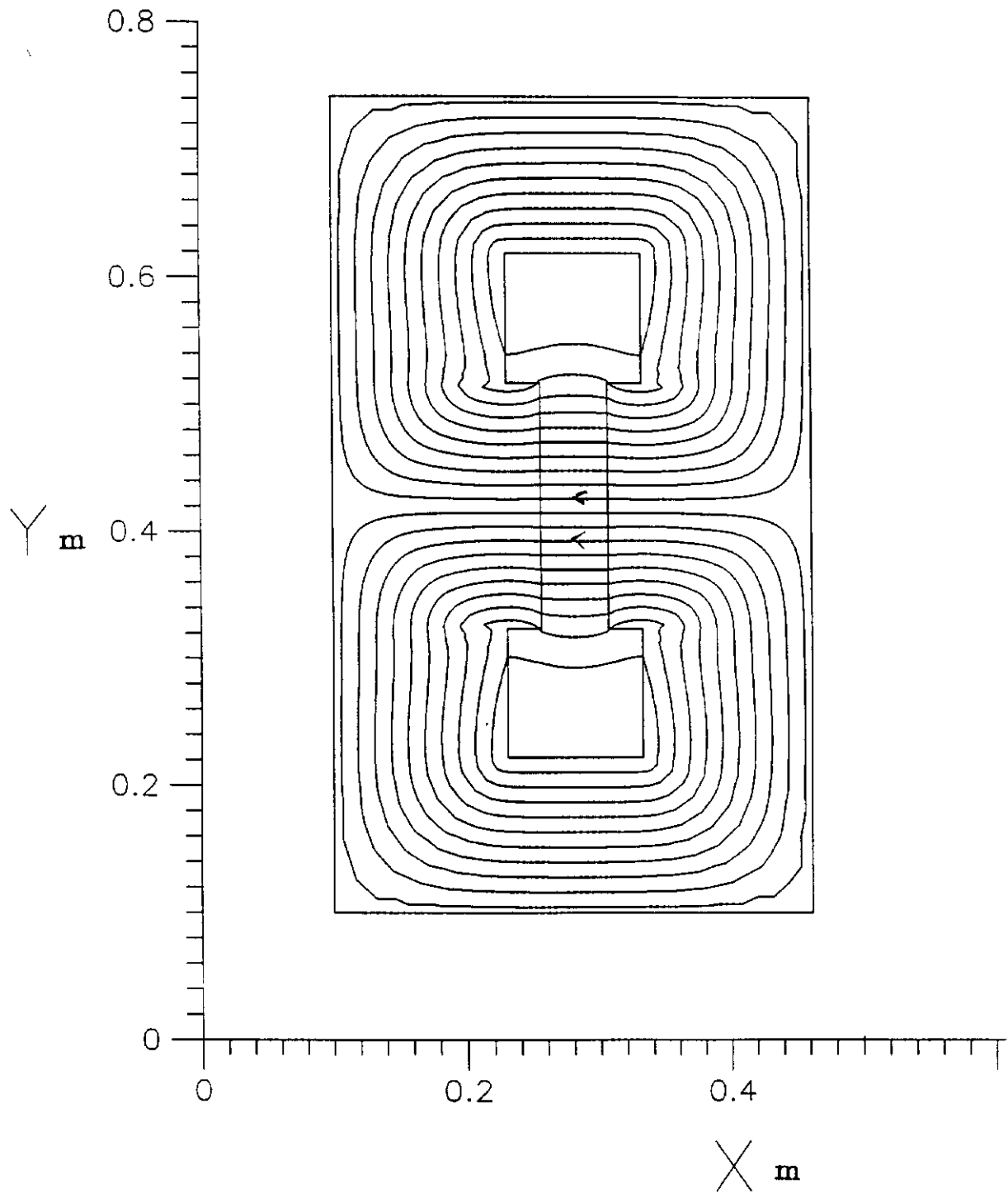


Figure 6: This figure is a cross-section of the magnet used in the third section of model 6) and 7). It is modeled after a Main-Ring dipole.

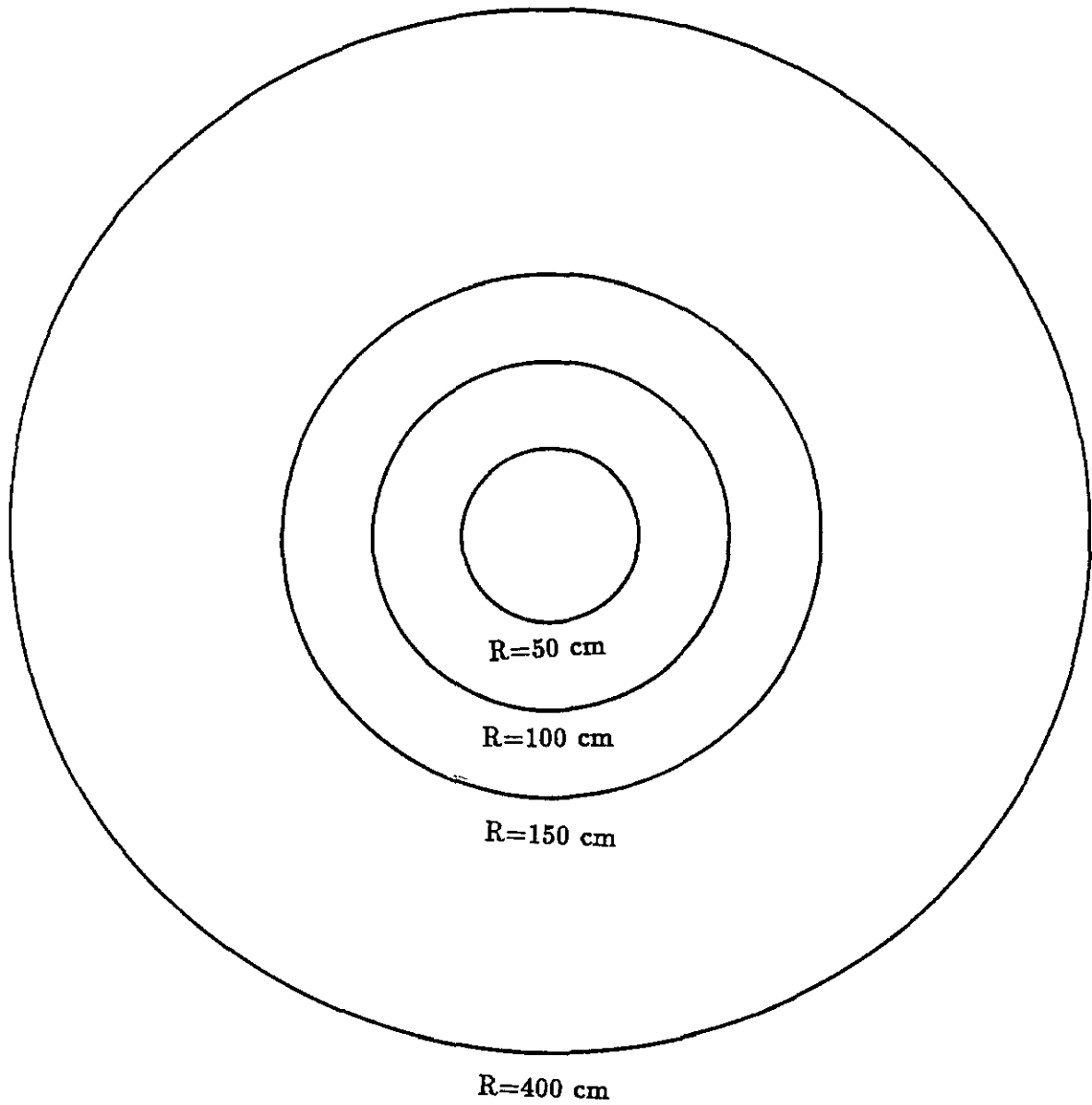


Figure 7: This figure shows the concentric rings which define the boundaries of the four regions into which the muon flux is divided.

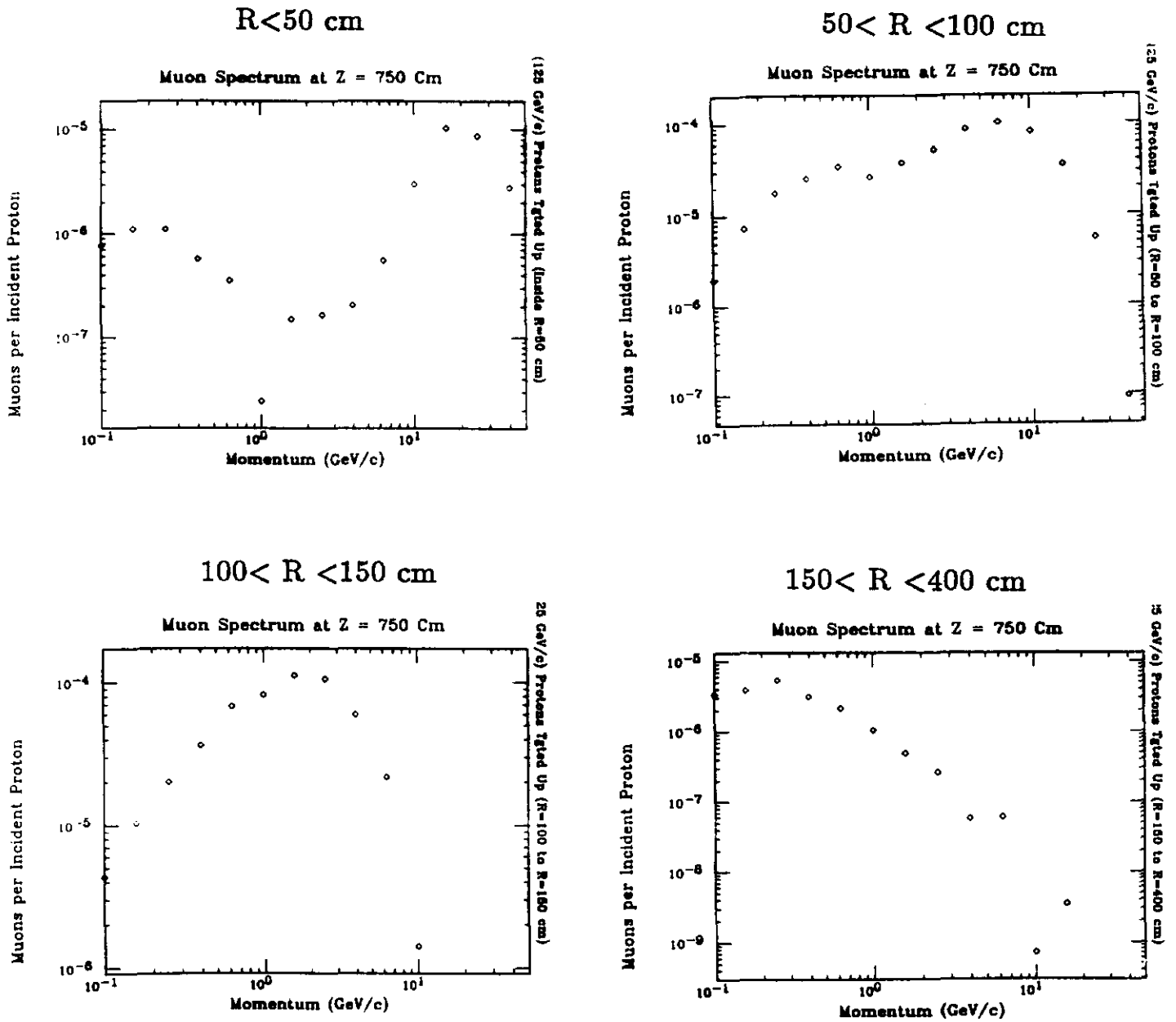


Figure 8: This figure shows the muon spectrum at the end of section 1 for the four regions. This spectrum was nearly identical for all of the models.

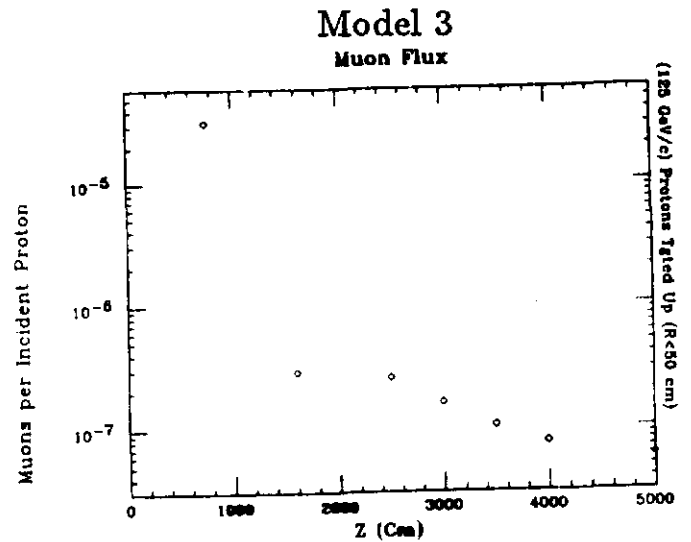
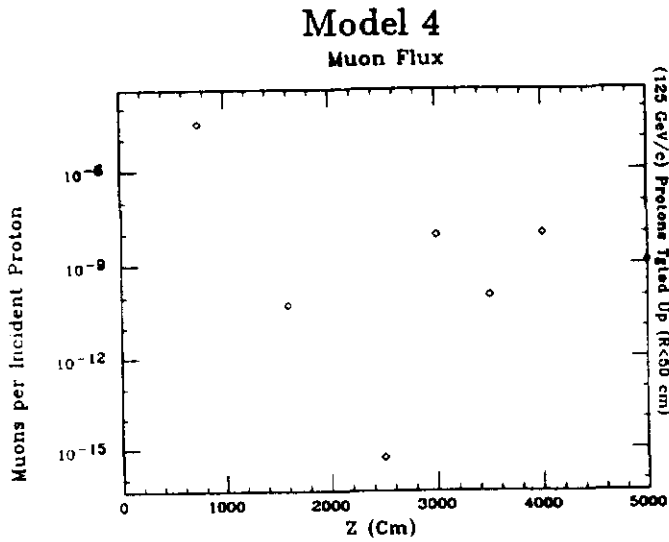
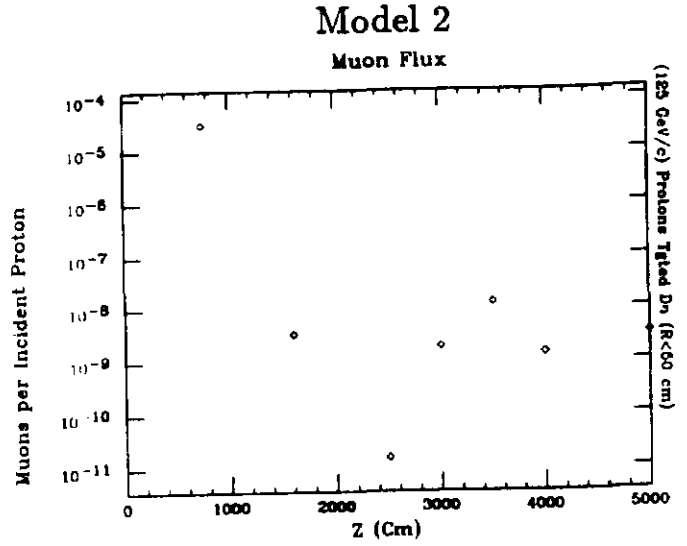
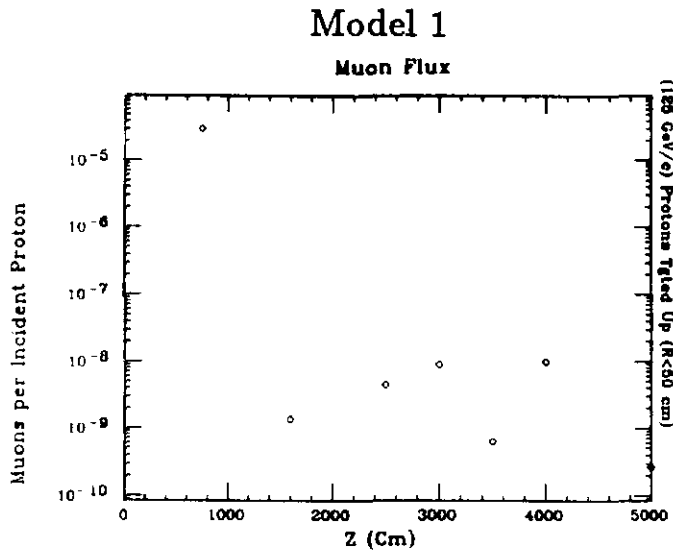


Figure 9: These plots show the results of models 1) to 4) inside the ring with radius 50 cm from the center of the neutral beam.

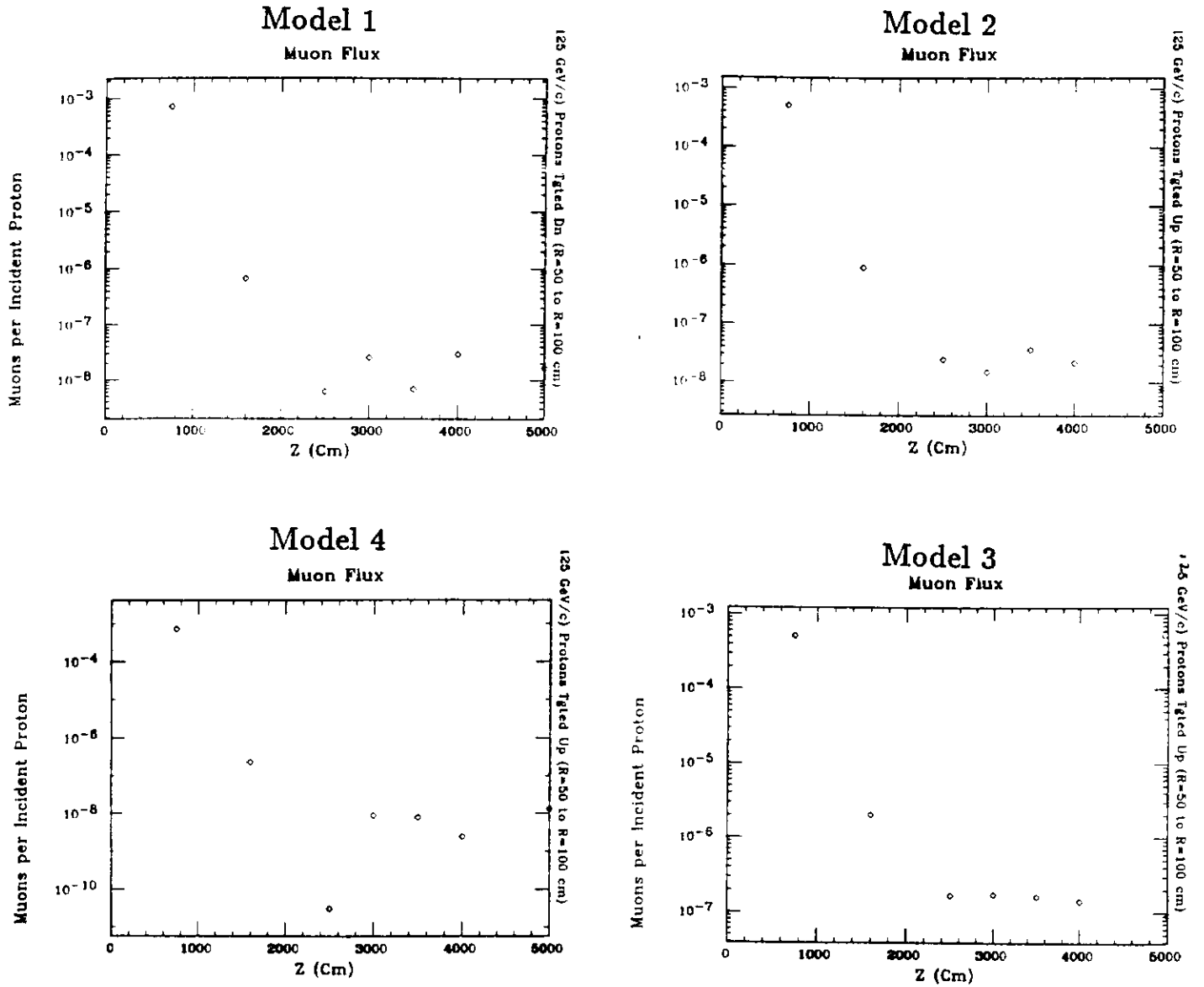


Figure 10: These plots show the results of models 1) to 4) in the region from 50 cm to 100 cm.

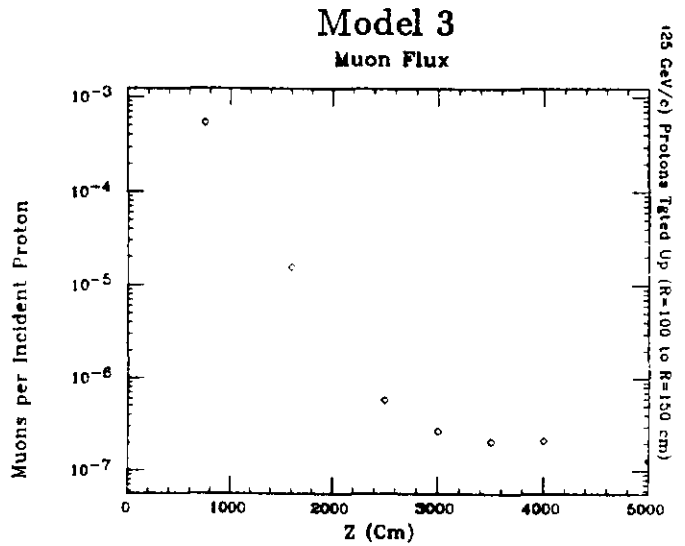
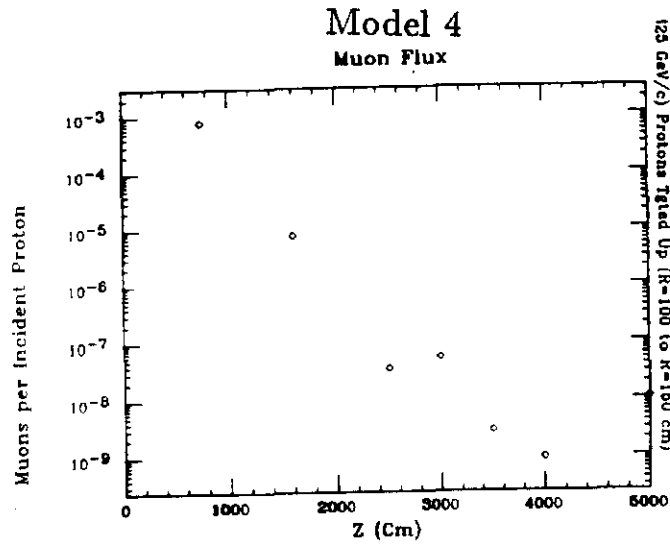
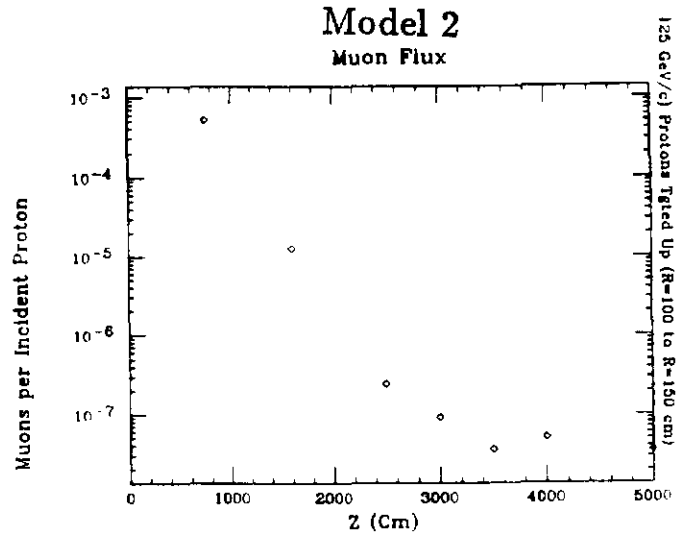
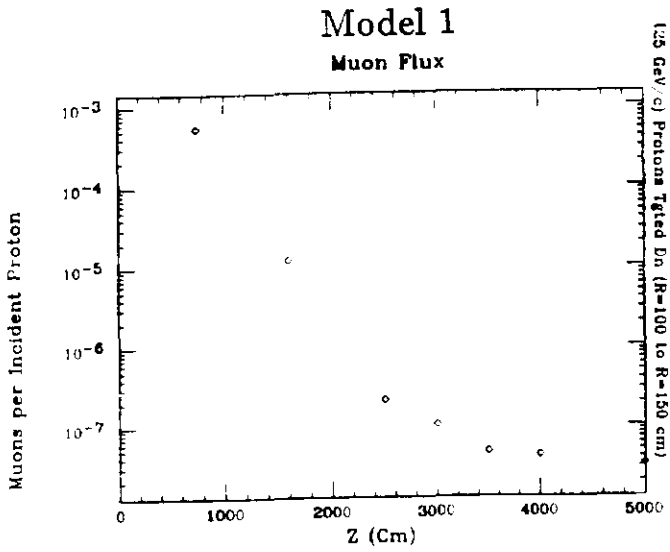


Figure 11: These plots show the results of models 1) to 4) in the region from 100 cm to 150 cm.

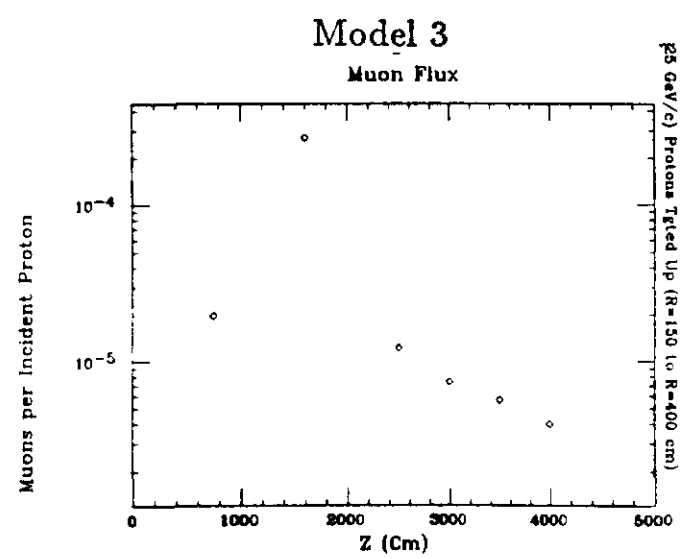
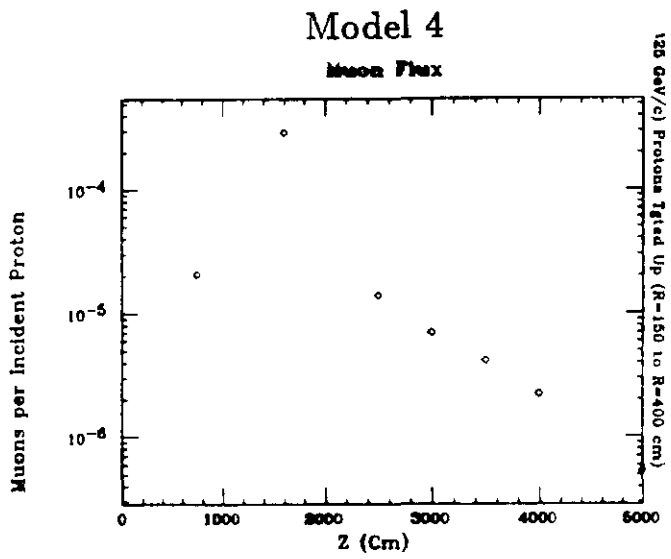
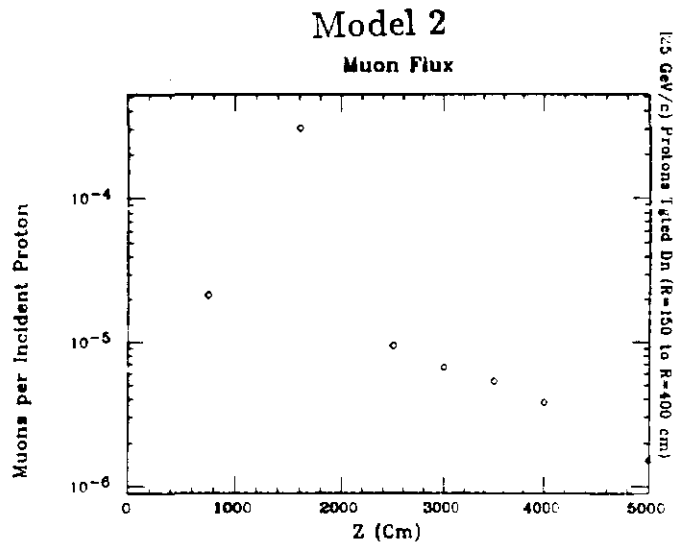
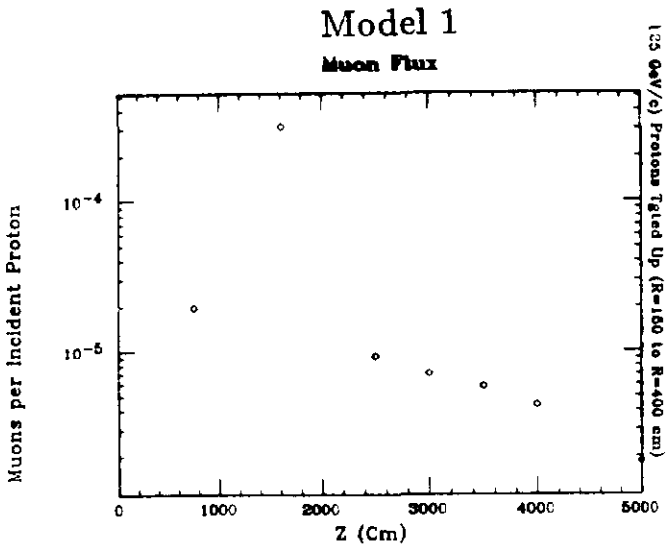


Figure 12: These plots show the results of models 1) to 4) in the region from 150 cm to 400 cm.

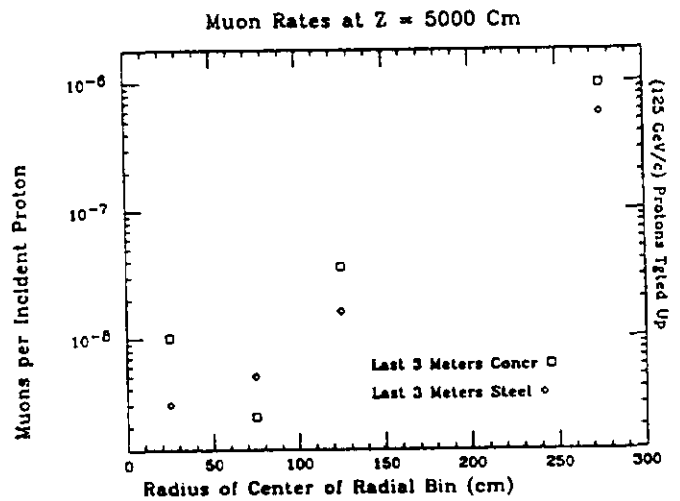
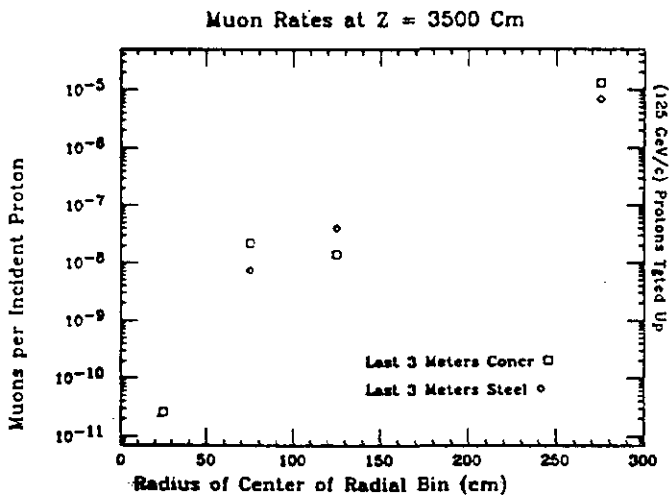
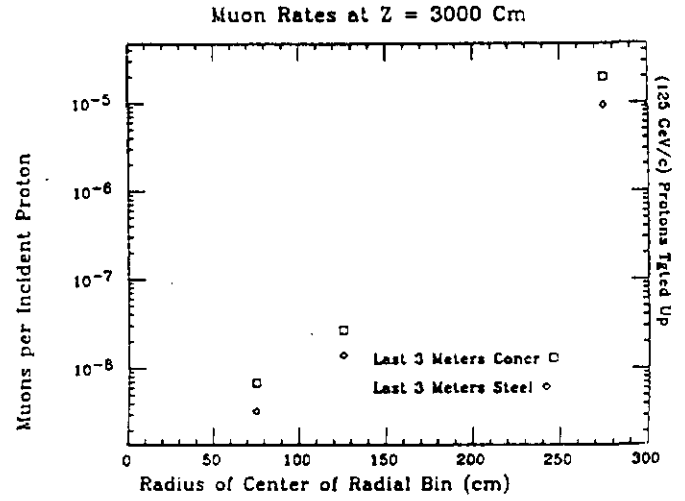
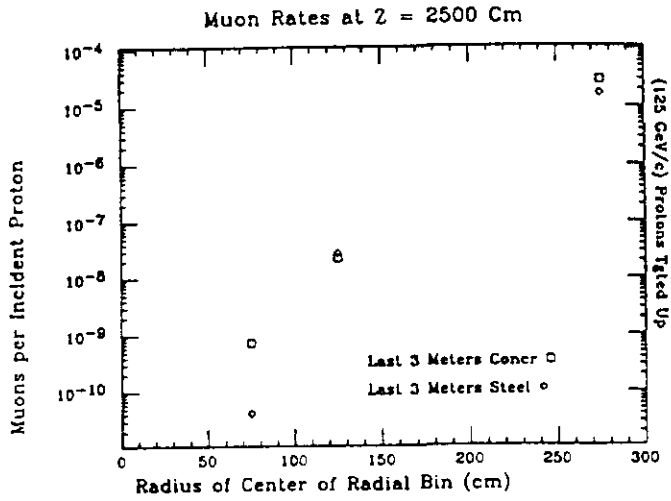


Figure 13: This plots compare the results of model 4) and model 5), where the last 3 meters of the third section were changed from inert steel to concrete.

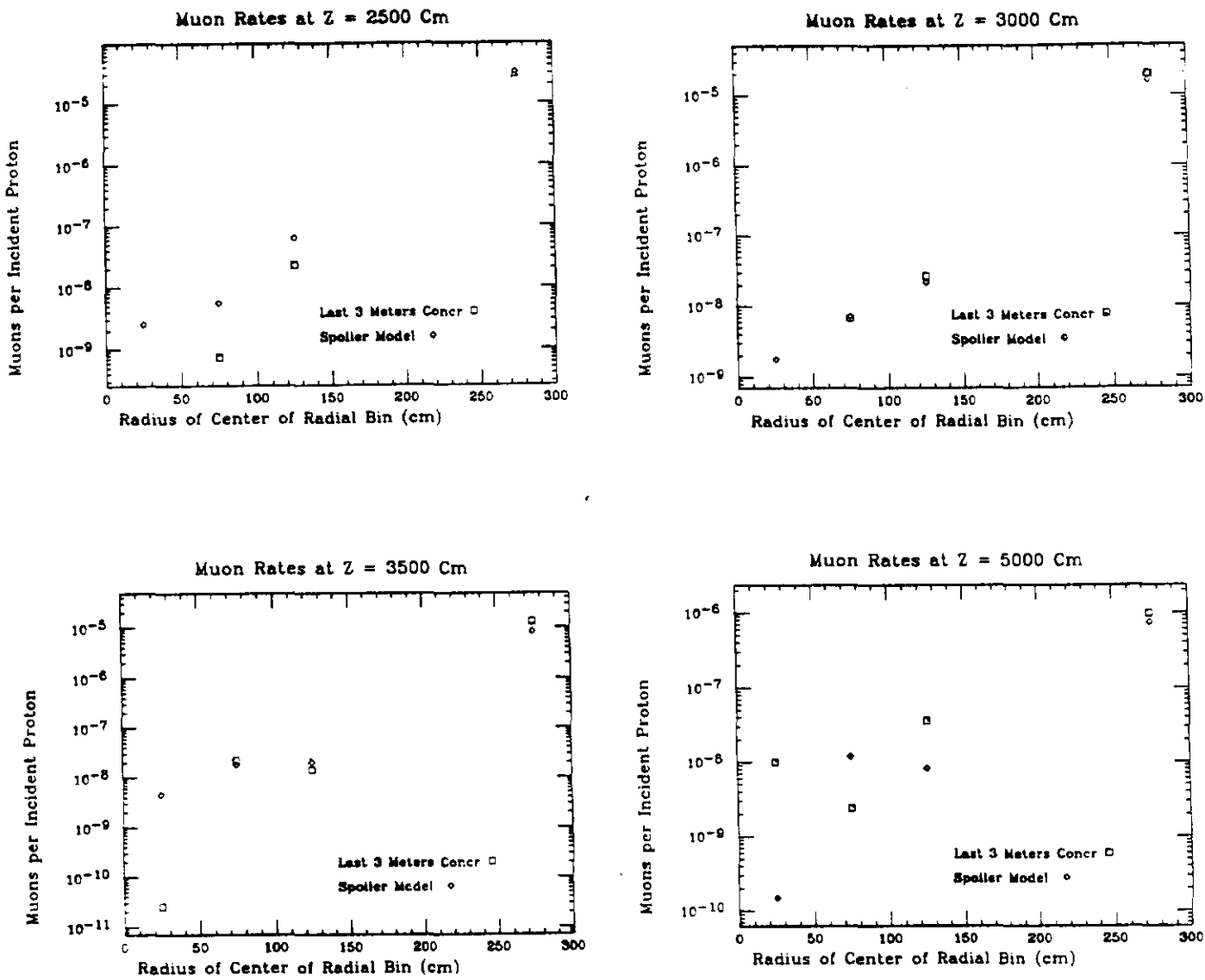


Figure 14: These plots compare the results of model 5) with model 6), the model with a large spoiler magnet in section 2 and a B2 dipole magnet in section 3.

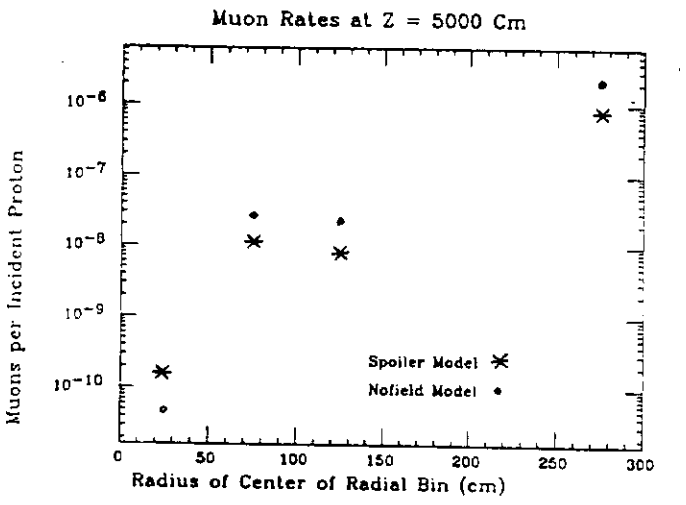
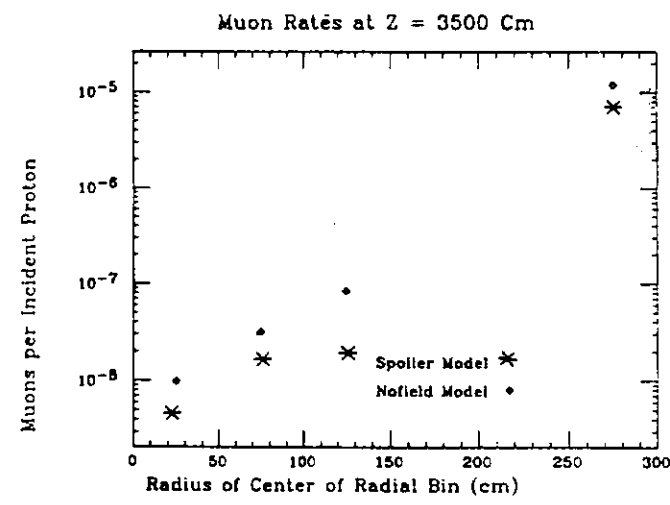
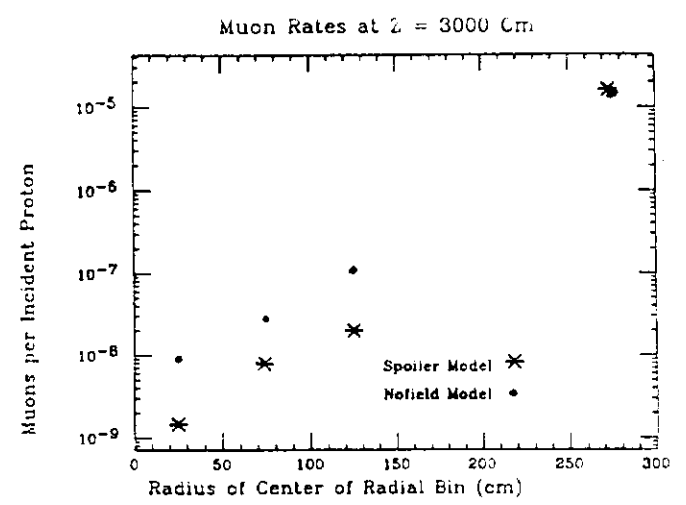
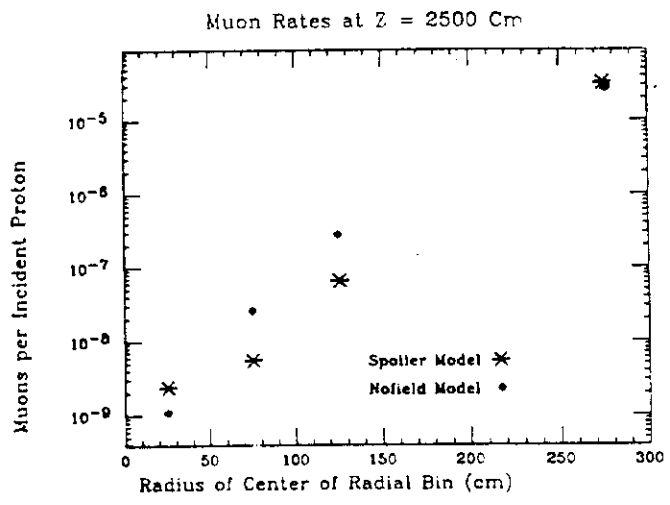


Figure 15: These plots compare the results of model 6) and model 7), where the magnetic field in the spoiler magnet of section 2 was set to zero.